Journal of the Physical Society of Japan **85**, 104401 (2016)
http://doi.org/10.7566/JPSJ.85.104401

Discrete Frequency Entangled Photon Pair Generation Based on Silicon Micro-ring Cavities

Jing Suo, Wei Zhang*, Shuai Dong, Yidong Huang, and Jiangde Peng

Tsinghua National Laboratory for Information Science and Technology, Department of Electronic Engineering, Tsinghua University, Beijing 100084, China

(Received May 5, 2016; accepted August 4, 2016; published online September 5, 2016)

In this paper, we propose and demonstrate a scheme to generate discrete frequency entangled photon pairs based on a silicon micro-ring resonator. The resonator is placed in a Sagnac fiber loop. Stimulated by two pump lights at two different resonance wavelengths of the resonator, photon pairs at another two resonance wavelengths are generated along two opposite directions in the fiber loop, by the nondegenerate spontaneous four wave mixing in the resonator. Their states are superposed and interfered at the output ports of the fiber loop to generate frequency entangled photon pairs. On the other hand, since the pump lights come from two continuous wave lasers, energy-time entanglement is an intrinsic property of the generated photon pairs. The entanglements on frequency and energy-time are demonstrated experimentally by the experiments of spatial quantum beating and Franson-type interference, respectively, showing that the silicon micro-ring resonators are ideal candidates to realize complex photonic quantum state generation.

1. Introduction

Silicon micro-ring resonators are important candidates to realize correlated and entangled photon pair generations through the spontaneous four wave mixing (SFWM).[1–6] In this process, two pump photons annihilate and two photons are generated simultaneously, the one with higher frequency named signal and the one with lower frequency named idler. Energy and momentum conservations are satisfied in the SFWM. Silicon micro-ring resonators have several advantages to perform photon pair generations. First of all, the third order nonlinear coefficient of silicon waveguides is about five orders higher than silica optical fibers, which makes it possible to realize photon pair generation on chip.[7,8] Secondly, the spectrum of spontaneous Raman scattering in silicon waveguides is narrow, hence it can be filtered out easily. Moreover, in the silicon micro-ring resonator, the pump lights and the generated signal and idler photons are all on resonance, it further enhances the nonlinearity. Based on the SFWM in a silicon micro-ring resonator, photon pair generations with different biphoton states have been demonstrated, including energy-time entanglement,[9,10] time-bin entanglement,[11] path entanglement,[12] and hyper-entanglement on polarization and energy-time.[13] Recently, the generation of frequency degenerate photon pairs is realized using a silicon micro-ring resonator, in which the signal and idler photons were separated in different paths and the Hong–Ou–Mandel (HOM) interference between them was demonstrated.[14,15]

In this paper we propose and demonstrate a generation scheme for the discrete frequency entanglement based on a silicon micro-ring resonator placed in a Sagnac fiber loop. The form of the discrete frequency entangled state could be expressed as $(|\omega_1\rangle_A|\omega_2\rangle_B + e^{i\phi}|\omega_1\rangle_B|\omega_2\rangle_A)/\sqrt{2}$, where ω_1 and ω_2 denote the frequencies of the generated photons, A and B denotes the two output ports of them and ϕ denotes the phase difference. On the other hand, since the pump lights come from continuous wave lasers, the generated photon pairs have the intrinsic property of energy-time entanglement. The properties of frequency and energy-time entanglement are demonstrated experimentally by the experiments of spatial quantum beating and Franson-type interference, respectively.

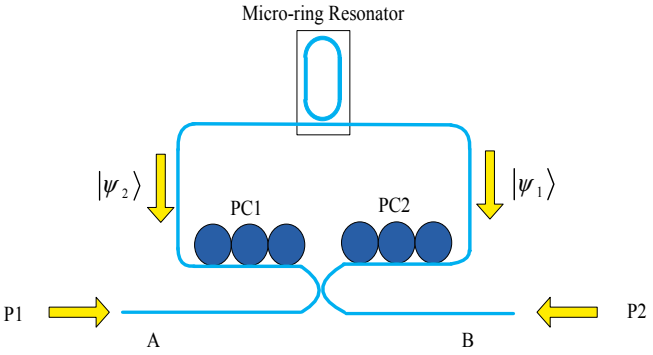

Fig. 1. (Color online) Sketch of the generation scheme of the frequency entanglement. PC: polarization controller.

2. Principle of the Scheme

The discrete frequency entangled biphoton state can be realized by the quantum interference between identical biphoton states with frequency correlation.[15–19] The micro-ring resonators have been demonstrated as ideal mediums to realize high quality biphoton states, in which the two photons are correlated at its two different resonance frequencies. While, the Sagnac fiber loop provides a stable setup for the quantum interference. Hence, placing the micro-ring resonator in a fiber Sagnac loop provides a feasible way to realize discrete frequency entanglement generation. The key point is the pumping scheme to realize the proper phase difference of the quantum interference.

The proposed scheme is shown in Fig. 1. The silicon micro-ring resonator is placed in a Sagnac fiber loop connected by a 50 : 50 fiber coupler. Considering that two pump lights with the same frequency would interfere at the 50 : 50 fiber coupler, which would lead to the unbalance of the pump lights along the two directions of the fiber loop, we use two pump lights with different frequencies, denoted by P1 and P2 in Fig. 1. They are injected into the Sagnac fiber loop from the ports A and B. Two polarization controllers

(PC1 and PC2) are used to adjust the polarization directions of the pump lights to stimulate the quasi-transverse electric (quasi-TE) mode of the waveguides in the silicon micro-ring resonator sample. Two biphoton states are generated in the silicon micro-ring resonator bidirectionally, propagate in clockwise (CW) and counter clockwise (CCW) directions in the Sagnac fiber loop, and interfere at the 50 : 50 fiber coupler. The two biphoton states before the interference can be described by $|\psi_1\rangle = |\omega_s\omega_i\rangle_{CW}$ and $|\psi_2\rangle = e^{i\Delta\varphi}|\omega_s\omega_i\rangle_{CCW}$, where $|\Psi_1\rangle$ and $|\Psi_2\rangle$ are correlated biphoton states generated in the CW and CCW directions, respectively, and $\Delta\varphi$ is their phase difference. ω_s and ω_i are the frequencies of the generated signal and idler photons, respectively.

The result of the interference is[14,17,18)]

$$|\Psi\rangle_{out} = \frac{1-e^{i\Delta\varphi}}{2} \times \frac{|\omega_s\rangle_A|\omega_i\rangle_A + |\omega_s\rangle_B|\omega_i\rangle_B}{\sqrt{2}} + \frac{i(1+e^{i\Delta\varphi})}{2} \times \frac{|\omega_s\rangle_A|\omega_i\rangle_B + |\omega_s\rangle_B|\omega_i\rangle_A}{\sqrt{2}}, \quad (1)$$

which is the state of the signal and idler photons outputting from the Sagnac fiber loop at the ports A and B.

In the SFWM process, the phase of the generated biphoton state is determined by the sum of the phases of the two annihilated pump photons. Hence, $\Delta\varphi = \Delta\varphi_{P1} + \Delta\varphi_{P2}$, where $\Delta\varphi_{P1}$ is the phase differences when the pump light P1 propagates along CW and CCW directions, and $\Delta\varphi_{P2}$ is that for the pump light P2. It can be seen that, what really matters in this scheme is the sum of the phase differences when the two pump lights pass through or cross the 50 : 50 fiber coupler, while the phase relationship between the two pump lights is not crucial. If the two pump lights are injected into the Sagnac fiber loop from the same port, e.g., Port A, the 50 : 50 fiber coupler would introduce an additional phase difference of $\pi/2$ between the light propagating along the CCW and CW directions for both of the pump lights, leading to $\Delta\varphi_{P1} = \Delta\varphi_{P2} = \pi/2$. In this case, $\Delta\varphi = \pi$ and the output state would be $(|\omega_s\rangle_A|\omega_i\rangle_A + |\omega_s\rangle_B|\omega_i\rangle_B)/\sqrt{2}$. It is a bunching state in which the signal and idler photons would output from the same port.

To realize frequency entanglement generation, we inject the two pump lights into the Sagnac fiber loop from the port A and B, respectively. In this case, the additional phase differences of the two pump lights introduced by the 50 : 50 coupler have different signs, i.e., $\Delta\varphi_{P1} = \pi/2$ and $\Delta\varphi_{P2} = -\pi/2$. They compensate for each other, leading to $\Delta\varphi = 0$. Hence, the output state would be $(|\omega_s\rangle_A|\omega_i\rangle_B + |\omega_i\rangle_B|\omega_i\rangle_A)/\sqrt{2}$. It is an anti-bunching state, in which the signal and idler photons would be output from different ports. If the frequencies of the signal and idler photons (ω_s and ω_i) are different, the state of $(|\omega_s\rangle_A|\omega_i\rangle_B + |\omega_i\rangle_B|\omega_i\rangle_A)/\sqrt{2}$ would be discrete frequency entangled state. Similar scheme has been used to realize a quantum splitter of frequency-degenerate photon pairs,[14)] in which the signal and idler photons generated at the same resonance are selected. In this paper, we select signal and idler photons generated at different resonances to realize the frequency entanglement generation.

It is worth noting that in the design of the experiment setup, the impact of fiber dispersion in the Sagnac fiber loop should be considered.[16)] The fiber lengths between the chip and the fiber coupler should be the same [assuming that the pigtails of the fiber coupler, the fiber polarization controller and the lensed fibers are all single mode fibers (SMF) with the same dispersion value] to ensure $\Delta\varphi = 0$. Hence, a fiber Sagnac loop with symmetric structure is required in this scheme.

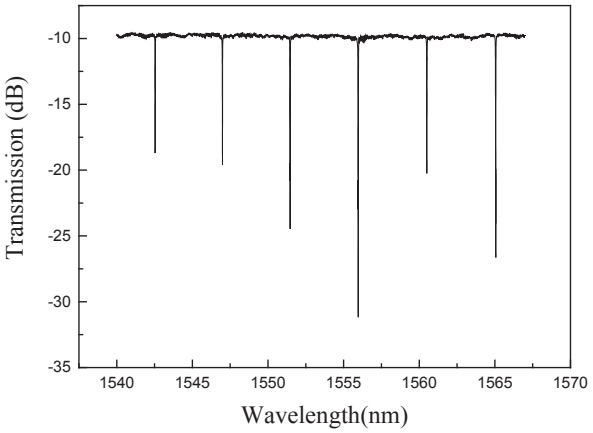

Fig. 2. Transmission spectrum of the bus waveguide and the silicon micro-ring resonator.

On the other hand, in this scheme both pump lights are generated by continuous wave lasers. The coherence times of the two pump lights are all much longer than the coherence times of the generated signal and idler photons, which are determined by the linewidths of the resonances for them. As a result, energy-time entanglement is an intrinsic property of the generated photon pairs, which is also demonstrated in the following experiment.[20,21)]

3. Experiment Setup

The silicon micro-ring resonator used in this experiment is fabricated using silicon-on-insulator substrate (by International Microelectronic, IME). The height and width of the waveguide in the resonator are 220 and 450 nm, respectively. The resonator has a racetrack shape with a perimeter of 132.5 μm. A bus waveguide of 5 mm in length couples with it. The transmission spectrum of the bus waveguide and the resonator is measured by a tunable laser (Santec TSL510) and shown in Fig. 2. The insertion loss of the bus waveguide (including the transmission loss and the coupling losses between the waveguide and the lensed fibers) is about 10 dB. The dips in the spectrum show the resonances. The parameters of the selected resonances used in this experiment are shown in Table I.

It is well known that the waveguide dispersion in the micro-ring resonator would lead to unequal frequency spaces between the adjacent resonances, which may impact the phase matching condition of the SFWM in the resonator and reduce its efficiency. According to the measured parameters in Table I, the difference between the sum of the resonance frequencies for the two pump lights ($f_{P1} + f_{P2}$) and that for the signal and idler photons ($f_s + f_i$) is about 2.8 GHz, which is well smaller than the 3 dB linewidths of the resonances for signal and idler photons (about 6.2 GHz). Hence, it can be expected that the SFWM would generate efficiently since the phase matching condition would be satisfied approximately.

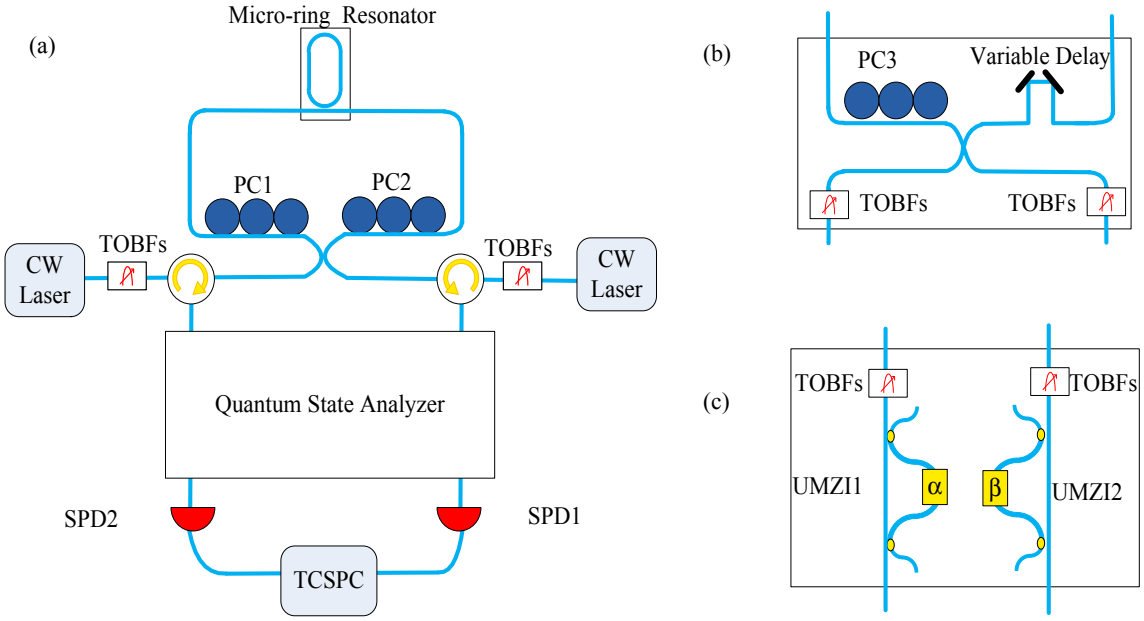

Fig. 3. (Color online) Experiment setup. (a) the main part. (b) the quantum state analyzer for frequency entanglement. (c) the quantum state analyzer for energy-time entanglement. TOBF: tunable optical band-pass filter, UMZI: unbalanced Mach–Zehnder interferometer, SPD: single photon detector, TCSPC: time correlated single photon counter.

Table I. Parameters of the selected resonances for the pump lights and the signal/idler photons.

	Resonance			
	for P1	for P2	for signal photons	for idler photons
Wavelength (nm)	1551.50	1556.00	1542.58	1565.08
3 dB linewidth (nm)	0.0075	0.0087	0.0085	0.0075
Extinction ratio (dB)	15	22	9	16
Quality factor	$\sim 2.1 \times 10^5$	$\sim 1.8 \times 10^5$	$\sim 1.8 \times 10^5$	$\sim 2.1 \times 10^5$

The experiment setup for the entanglement generation is shown in Fig. 3. Figure 3(a) shows the main part. Two pump lights are generated by two tunable continuous wave lasers at 1551.5 and 1556 nm, respectively, and then pass through tunable optical bandpass filters (TOBFs) to suppress their spontaneous emissions near the resonances for the signal and idler photons. Circulators are used to guide the pump lights into the Sagnac fiber loop. The Sagnac fiber loop composes of a 50 : 50 fiber coupler, a manual alignment system to couple the pump lights into the micro-ring resonator sample through lensed fibers, and two polarization controllers (PC1 and PC2) to match the pump lights to the quasi-TE mode of the waveguides in the sample. The fiber lengths between the chip and the 50 : 50 coupler of the two sides are almost the same, the difference is no more than 10 cm. Photon pairs are generated in the resonator and propagate in Sagnac fiber loop along the CW and CCW directions, respectively. The photons from the Sagnac fiber loop are directed to two single photon detectors (SPD1 and SPD2, Id220, IDQ Inc) through the two circulators and a quantum state analyzer. The detection efficiencies of the two single photon detectors are set at 10%. The results of the single photon detectors are sent to a time correlated single photon counter (TCSPC; Becker & Hickl DPC-230) for the coincidence counting.

The quantum state analyzer shown in Fig. 3(a) is used to demonstrate the property of entanglement, which has different setup for the entanglement on different freedom. The frequency entanglement is demonstrated by the spatial quantum beating. The quantum state analyzer for this experiment is shown in Fig. 3(b). The output photons from ports A and B are directed to a 50 : 50 fiber coupler by two paths. On one path, a variable delay line is used to tune the length difference of the two paths. On the other path, a polarization controller (PC3) is used to maximize the quantum interference. After the 50 : 50 fiber coupler, TOBFs are used to select signal and idler photons, respectively. On the other hand, the energy-time entanglement is demonstrated by the Franson-type interference with a quantum state analyzer shown in Fig. 3(c). The signal and idler photons are firstly selected by TOBFs on the two ports, respectively, and then directed to two unbalance Mach–Zehnder interferometers (Kylia UMZI1 and UMZI2, mint-1 × 2-L-2.5 GHz) to realize quantum interference. The UMZI has a time delay of 400 ps between its two arms and the phase difference between the two arms can be tuned by the electric voltage applied on it. The phase differences of UMZI1 and UMZI2 are denoted by α and β, respectively.

4. Experiment Results of the Entanglement Generation

4.1 The property of photon pair generation

First of all, we measure the property of photon pair generation in the experiment setup shown in Fig. 3. The quantum state analyzer is not necessary in this measurement. The output photons at the ports A and B are directed to the two SPDs through two TOBFs, by which SPD1 and SPD2 detect signal photons and idler photons, respectively. Both the single side photon counts (signal side) and the coincidence to accidental coincidence count ratio (CAR) are measured under different pump levels. In the experiment, the two pump lights always have the same power. Hence, we use the power of one of them to indicate the pump level. The experimental results are shown in Fig. 4. The red squares are

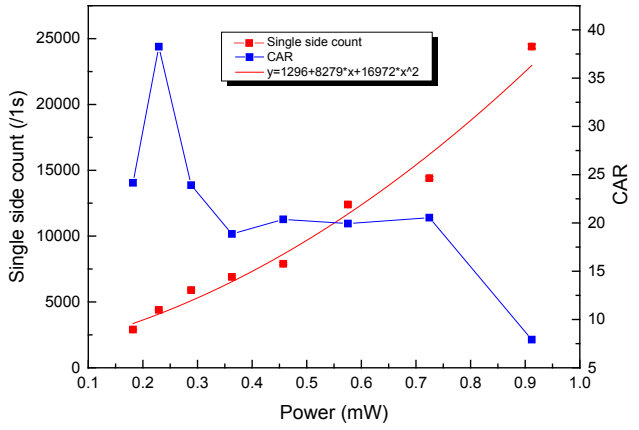

Fig. 4. (Color online) The experiment results of signal side photon count rate and CAR under different pump levels.

the results of the signal side photon count rate. It can be seen that the signal side photon count rate rises with increasing pump level. The red line is their fitting curve using $y = Ax^2 + Bx + C$. The contribution of the quadratic term is obvious, showing that photon pairs generate effectively in the resonator by the SFWM. The linear term may be due to the spontaneous Raman scattering in the fibers when the pump lights propagates in the experiment setup, while, the linear term is due to the dark counts of the SPD. The blue squares show the result of CAR. In most pump levels we used in the experiment, the CAR increases with decreasing pump level. While, it drops when the power for each pump light is lower than 0.2 mW. The maximum CAR is close to 40. The CAR is around 20 when the pump level is set at 0.3–0.7 mW. The measured CAR in this setup is relatively low compared with our previous works about correlated/entangled photon pair generation based on silicon micro-ring resonators.[6,13] It is mainly due to the unwanted noise photons generated by the degenerate SFWM stimulated by one pump light. While, the measured CAR is sufficient to demonstrate the frequency entanglement.

4.2 Demonstration of the discrete frequency entanglement

To demonstrate the property of frequency entanglement, the quantum state analyzer shown in Fig. 3(b) is used to realize the experiment of spatial quantum beating.[22,23] The pump level is set to support a signal side count rate of about 7 kHz. The coincidence counts are recorded under different time delays introduced by the variable delay line.

According to the theoretical analysis about the spatial quantum beating,[23] the fringe can be expressed as

$$y = A[1 - Vf(t)\sin(\omega_2\tau + c)], \quad (2)$$

where V is the fringe visibility of the spatial quantum beating. ω_2 is the frequency difference between the signal an idler photons. $f(t)$ is a normalized function decided by the spectra of the signal and idler photons. In the experiment, the spectra of the signal and idler photons are determined by the spectra of their corresponding resonances,[23] which have Lorentzian shapes. Hence, $f(t)$ can be approximated by an exponential function, $f(t) = \exp(-\omega_1\tau)$, where ω_1 can be calculated by the average spectral width of the resonances for generated photon pairs. c represents the initial phase of the beating fringe, which is determined by the delay between the two arms.

Since the spectral widths of the signal and idler photons are quite narrow and their frequency difference is relatively large. It can be expected that the fringe would have a small period and a broad envelope. Hence, we did not measure the whole fringe, but measure it under three typical time delays. Figure 5(a) shows the experiment results and their fitting fringe according to Eq. (2). The details of the results under the three typical time delays are shown in Figs. 5(b), 5(c), and 5(d), respectively. It can be seen that under all the three time delays, the fitting fringes agree with the experiment results very well.

The raw visibility of the fringe is $66.7 \pm 3.4\%$, while it reaches $75.0 \pm 3.8\%$ after subtracting the accidental coincidence count. The fitting values of ω_1 and ω_2 are $2\pi \times 0.99$ GHz and $2\pi \times 2805$ GHz, respectively. They agree well with the calculated values of ω_1 and ω_2 ($2\pi \times 1.00$ GHz and $2\pi \times 2809$ GHz, respectively), in which ω_1 is calculated by the average linewidth of the resonances, which is 0.008 nm according to Table I, and ω_2 is calculated according to the frequency difference of the two resonances for the signal and idler photons. The clear spatial quantum beating fringe demonstrates the property of frequency entanglement. It is worth noting that the strong back scattering in the silicon micro-ring resonator due to the roughness of the waveguide side walls could make the powers of the pump lights propagating in CW and CCW directions unbalanced.[24,25] They may also impact the fringe visibility. On the other hand, the fringe visibility is sensitive to the polarization states of the pump lights and signal/idler photons. Carefully adjustments are required on the three fiber polarization controllers (PC1, PC2, and PC3) to improve the fringe visibility.

It is worth noting that the coincidence count rate in the experiment is relatively low, which may also limit the fringe visibility. It is mainly due to the limited collection efficiencies of the experiment setup. The factors impact the collection efficiencies include the coupling losses between the lensed fibers and the silicon waveguides (~5 dB/facet), the limited SPD efficiency (10%), the losses of signal/idler filters (~3 dB) and losses due to other optical components in the setup (~3 dB). Better results could be expected if the coupling method of silicon chip is improved and SPDs with higher performance are used.[26]

4.3 Demonstration of the energy-time entanglement

Since we use continuous wave lasers to generate the pump lights, energy-time entanglement is an intrinsic property of the generated photon pairs. We also demonstrate it experimentally. To demonstrate the property of energy-time entanglement, the quantum state analyzer shown in Fig. 3(b) is used to realize the Franson-type interference. In this experiment, the detection efficiency of the two SPDs are set at 20%. The signal side photon count rate is also about 7 kHz.

A typical coincidence count result is shown in Fig. 6. It can be seen that there are three peaks in the histogram recorded by the TCSPC equipment due to the arm length differences of the two UMZIs. The central coincidence peak is contributed by two cases, corresponding to the case that both photons pass through the long arms of the UMZIs and that both photons pass through the short arms of the UMZIs,

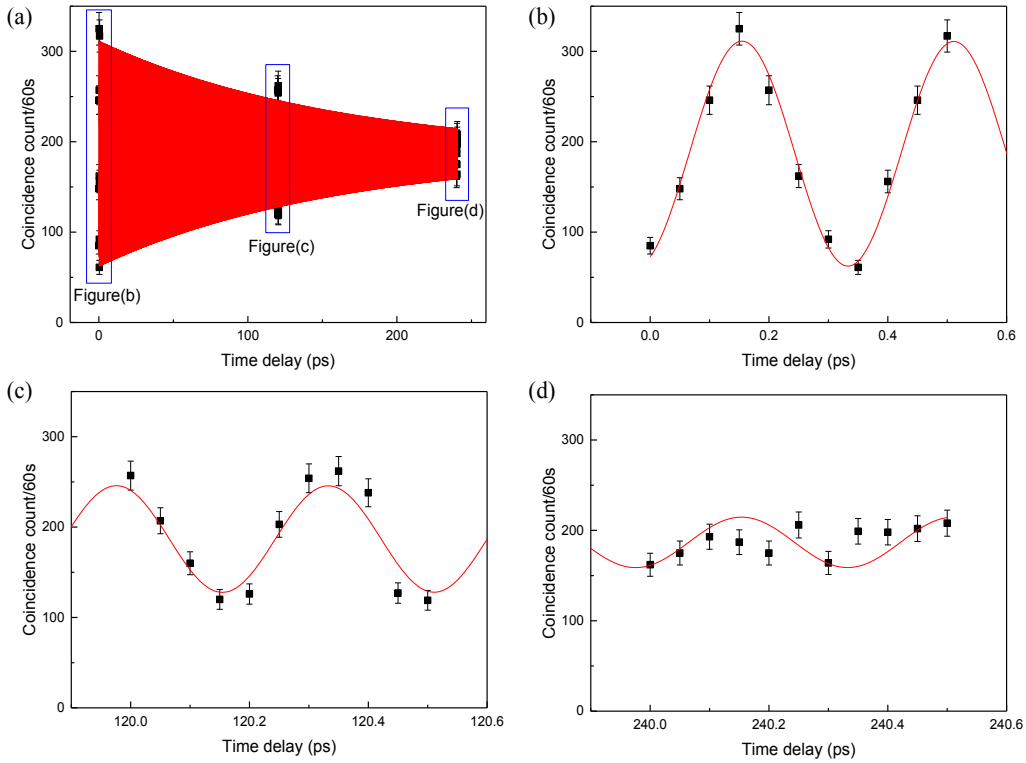

Fig. 5. (Color online) (a) The measured fringe of the spatial quantum beating and their fitting curve. (b)–(d) The experiment result under time delays of (b) 0, (c) 120, and (d) 240 ps.

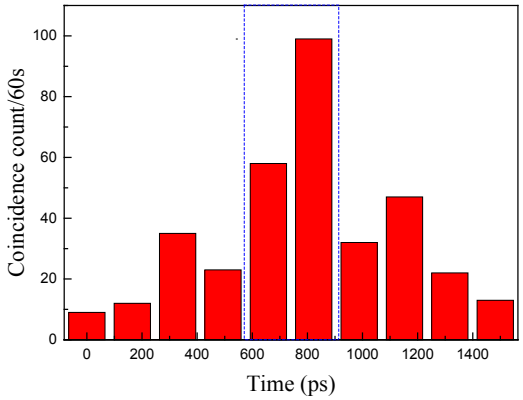

Fig. 6. (Color online) A typical coincidence count record in the experiment of the Franson-type interference.

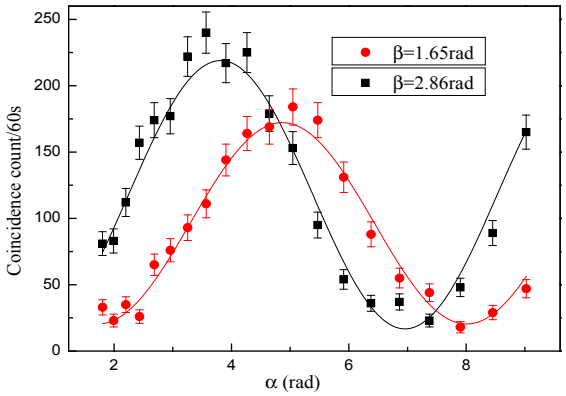

Fig. 7. (Color online) The measured fringes in the experiment of the Franson-type interference. The red solid circles: the fringe measured when $\beta = 1.65$; The black squares: the fringe measured when $\beta = 2.86$ rad; The solid lines: the fitting curves of the fringes.

respectively. The two cases are indistinguishable and their states are coherently superposed, showing the property of energy-time entanglement. As a result, the central coincidence peaks show an interference fringe under varying relative phase differences of the UMZIs. In the experiment, we take each record in 60 s and extract the coincidence counts from two time bins covering the central peak, which is marked between the dashed lines in Fig. 6. The accidental coincidence counts are defined by the average coincidence counts in the two bins out of the peaks and the average is calculated by the coincidence counts of 5000 time bins. Due to the limitation of the arm length differences of the UMZIs used in the experiment, the three peeks are a little close, however, it is enough to demonstrate the energy-time entanglement.

The measurement results of the interference fringes are shown in Fig. 7. The red points and black squares are the experiment results under different α when β is set at 1.65 and 2.86 rad, respectively. The red and black lines are their fitting curves. It can be seen that the raw visibilities of the two fringes are 78.8 ± 2.6 and $85.8 \pm 3.5\%$, respectively. Both of the visibilities are higher than $1/\sqrt{2}$, the benchmark for the violation of Bell's inequality. After deducting the accidental coincidence count, their net visibilities reach 89.7 ± 2.6 and $95.3 \pm 3.5\%$, respectively. Hence, the energy-time entanglement is demonstrated. Due to the variations of the alignment condition and the light polarization in the loop, there is a visibility difference about 7% between the two fringes.

5. Conclusion

In this paper, we propose a generation scheme for the discrete frequency entanglement based on a silicon micro-ring resonator. The silicon micro-ring resonator is placed in a Sagnac fiber loop and stimulated by two pump lights at two different resonance wavelengths, which inject into the Sagnac fiber loop from different input ports. The biphoton states generate in the resonator, propagate along the CW and CCW direction in the Sagnac fiber loop respectively and interfere at the 50 : 50 fiber coupler, leading to an anti-bunching biphoton state generation. This state is a discrete frequency entangled state if the signal and idler photons generated in two different resonances are selected by proper optical filtering. Since in this scheme continuous wave lasers are used as the two pump lights, the generated photon pairs have intrinsic property of energy-time entanglement. This scheme is demonstrated experimentally. The property of the discrete frequency entanglement is demonstrated by the experiment of spatial quantum beating. The raw visibility of the measured fringe is $66.7 \pm 3.4\%$. The property of energy-time entanglement is demonstrated by the Franson-type interference. The raw visibilities of the fringes measured under $\beta = 1.65$ and 2.86 rad are 78.8 ± 2.6 and $85.8 \pm 3.5\%$, respectively. The experiment results show that this scheme is promising on realizing entanglement on frequency and energy-time, which extends the applications of the silicon micro-ring resonators on the generations of complex photonic quantum states.

Acknowledgments

This work was supported by 973 Programs of China under Contract Nos. 2013CB328700 and 2011CBA00303, the National Natural Science Foundation of China under Contract Nos. 61575102 and 61321004, Tsinghua University Initiative Scientific Research Program under Contract No. 20131089382.

*zwei@tsinghua.edu.cn

1) S. Azzini, D. Grassani, M. Galli, L. C. Andreani, M. Sorel, M. J. Strain, L. G. Helt, J. E. Sipe, M. Liscidini, and D. Bajoni, Opt. Lett. **37**, 3807 (2012).
2) S. Clemmen, K. P. Huy, W. Bogaerts, R. G. Baets, P. Emplit, and S. Massar, Opt. Express **17**, 16558 (2009).
3) S. Azzini, D. Grassani, M. J. Strain, M. Sorel, L. G. Helt, J. E. Sipe, M. Liscidini, M. Galli, and D. Bajoni, Opt. Express **20**, 23100 (2012).
4) E. Engin, D. Bonneau, C. M. Natarajan, A. S. Clark, M. G. Tanner, R. H. Hadfield, S. N. Dorenbos, V. Zwiller, K. Ohira, N. Suzuki, H. Yoshida, N. Iizuka, M. Ezaki, J. L. O'Brien, and M. G. Thompson, Opt. Express **21**, 27826 (2013).
5) L. G. Helt, Z. Yang, M. Liscidini, and J. E. Sipe, Opt. Lett. **35**, 3006 (2010).
6) Y. Guo, W. Zhang, N. Lv, Q. Zhou, Y. Huang, and J. Peng, Opt. Express **22**, 2620 (2014).
7) N. C. Harris, D. Grassani, A. Simbula, M. Pant, M. Galli, T. Baehr-Jones, M. Hochberg, D. Englund, D. Bajoni, and C. Galland, Phys. Rev. X **4**, 041047 (2014).
8) J. E. Sharping, K. F. Lee, M. A. Foster, A. C. Turner, B. S. Schmidt, M. Lipson, A. L. Gaeta, and P. Kumar, Opt. Express **14**, 12388 (2006).
9) D. Grassani, S. Azzini, M. Liscidini, M. Galli, M. J. Strain, M. Sorel, J. E. Sipe, and D. Bajoni, Optica **2**, 88 (2015).
10) R. Kumar, M. Savanier, J. R. Ong, and S. Mookherjea, Opt. Express **23**, 19318 (2015).
11) R. Wakabayashi, M. Fujiwara, K. Yoshino, Y. Nambu, M. Sasaki, and T. Aoki, Opt. Express **23**, 1103 (2015).
12) J. W. Silverstone, R. Santagati, D. Bonneau, M. J. Strain, M. Sorel, J. L. O'Brien, and M. G. Thompson, Nat. Commun. **6**, 7948 (2015).
13) J. Suo, S. Dong, W. Zhang, Y. Huang, and J. Peng, Opt. Express **23**, 3985 (2015).
14) J. He, B. A. Bell, A. Casas-Bedoya, Y. Zhang, A. S. Clark, C. Xiong, and B. J. Eggleton, Optica **2**, 779 (2015).
15) M. Fiorentino, P. L. Voss, J. E. Sharping, and P. Kumar, IEEE Photonics Technol. Lett. **14**, 983 (2002).
16) N. Zhao, L. Yang, and X. Li, Opt. Lett. **37**, 1220 (2012).
17) X. Li, L. Yang, X. Ma, L. Cui, Z. O. Ou, and D. Yu, Phys. Rev. A **79**, 033817 (2009).
18) J. W. Silverstone, D. Bonneau, K. Ohira, N. Suzuki, H. Yoshida, N. Iizuka, M. Ezaki, C. M. Natarajan, M. G. Tanner, R. H. Hadfield, V. Zwiller, G. D. Marshall, J. G. Rarity, J. L. O'Brien, and M. G. Thompson, Nat. Photonics **8**, 104 (2013).
19) B. Fang, O. Cohen, J. B. Moreno, and V. O. Lorenz, Opt. Express **21**, 2707 (2013).
20) J. Brendel, N. Gisin, W. Tittel, and H. Zbinden, Phys. Rev. Lett. **82**, 2594 (1999).
21) Q. Zhang, H. Takesue, S. W. Nam, C. Langrock, X. Xie, B. Baek, M. M. Fejer, and Y. Yamamoto, Opt. Express **16**, 5776 (2008).
22) S. Dong, L. Yu, W. Zhang, J. Wu, W. Zhang, L. You, and Y. Huang, Sci. Rep. **5**, 9195 (2015).
23) Z. Y. Ou and L. Mandel, Phys. Rev. Lett. **61**, 54 (1988).
24) F. Morichetti, A. Canciamilla, M. Martinelli, A. Samarelli, R. M. De La Rue, M. Sorel, and A. Melloni, Appl. Phys. Lett. **96**, 081112 (2010).
25) F. Ladouceur and L. Poladian, Opt. Lett. **21**, 1833 (1996).
26) A. Dutt, K. Luke, S. Manipatruni, A. L. Gaeta, P. Nussenzveig, and M. Lipson, Phys. Rev. Appl. **3**, 044005 (2015).